Modeling and Experimental Investigation of Rheological Properties of Injectable Poly(lactide ethylene oxide fumarate)/ Hydroxyapatite Nanocomposites

Alireza S. Sarvestani and Esmaiel Jabbari*

Biomimetic Materials and Tissue Engineering Laboratories, Department of Chemical Engineering, University of South Carolina, Columbia, South Carolina 29208

Received December 15, 2005; Revised Manuscript Received February 28, 2006

Injectable multiphasic polymer/ceramic composites are attractive as bioresorbable scaffolds for bone regeneration because they can be cross-linked in situ and are osteoconductive. The injectability of the composite depends on the nanoparticle content and the energetic interactions at the polymer/particle interface. The objective of this research was to determine experimentally the rheological properties of the PLEOF/apatite composite as an injectable biomaterial and to compare the viscoelastic response with the predictions of a linear elastic dumbbell model. A degradable in situ cross-linkable terpolymer based on low molecular weight poly(L-lactide) and poly(ethylene oxide) linked by unsaturated fumarate groups is synthesized. The poly(L-lactide-*co*-ethylene oxide-*co*-fumarate) (PLEOF) terpolymer interacts with the surface of the apatite nanoparticles by polar interactions and hydrogen bonding. A kinetic model is developed that takes into account the adsorption/desorption of polymer chains to/from the nanoparticle surface. Rheological properties of the aqueous dispersion of PLEOF terpolymer reinforced with nanosized hydroxyapatite (HA) particles are investigated using mechanical rheometry. To this end, we performed a series of rheological experiments on un-cross-linked PLEOF reinforced with different volume fractions of HA nanoparticles. The results demonstrate that the observed nonlinear viscoelasticity at higher shear rates is controlled by the energetic interactions between the polymer chains and dispersed particle aggregates and by the rate of the adsorption/desorption of the chains to/from the surface of the nanoparticles.

Introduction

Synthetic degradable biomaterials with a wide range of mechanical, biologic, degradation, and rheologic properties, embedded with osteoinductive factors, and seeded with multilineage progenitor cells provide an exciting approach to bone regeneration.[1,2] Injectable scaffolds are more suitable for treating irregularly shaped defects in applications such as vertebroplasty, unicameral bone cysts, and focal cartilage defects, where rigid scaffolds are more difficult to form into aberrant configurations.[3−8] Injectable multiphasic polymer/ceramic composites are an attractive option as a bioresorbable bone cement because they do not illicit an immune response, cross-link in situ to the desired mechanical properties, and are osteoconductive. Osteoinductive factors can be embedded in the polymer phase to facilitate the migration of cells to the scaffold.[9−13] An ideal multiphasic scaffold should have suitable rheological properties for injection, have maximum interfacial bonding between the polymer and ceramic phases, degrade concurrently with the extracellular matrix formation, and provide a medium for the release and diffusion of bioactive agents.[4,14]

Recently, our laboratory has developed an injectable hydrogel/apatite nanocomposite that can be cross-linked in situ using a neutral redox initiation system.[15] The hydrogel phase is a poly(lactide-*co*-ethylene oxide-*co*-fumarate) (PLEOF) terpolymer consisting of low molecular weight poly(L-lactide) (PLA) and poly(ethylene glycol) (PEG) blocks linked by unsaturated fumarate units.[16] The water content and mesh-size of the hydrogel can be adjusted by the ratio of the hydrophilic PEG to hydrophobic PLA blocks and by the molecular weight of PEG. The network density can be controlled by the density of fumarate groups on the terpolymer chains. We have demonstrated that the apatite nanoparticles can be grafted with unsaturated groups for inter-cross-linking with the hydrogel phase to maximize interfacial bonding.[17−19] A peptide cross-linker which is degradable enzymatically by matrix metalloproteinases is used to chemically bond the hydrogel and apatite phases into a solid three-dimensional network.[20] We have demonstrated that the PLEOF/apatite nanocomposite supports attachment and migration of marrow stromal cells isolated from the bone marrow.[20]

The objective of this research was to determine experimentally the rheological properties of the PLEOF/apatite composite as an injectable biomaterial for bone regeneration and to compare the non-Newtonian rheological response with a linear elastic dumbbell model. There are significant energetic interactions between the polar ethylene oxide units of the hydrogel phase and the ionic groups of the apatite nanoparticles, resulting in shear thinning and reduction in shear storage modulus at higher amplitudes of oscillation. This phenomenon, often referred to as the Payne effect,[21] has been observed in polymer/ceramic composites and extensively studied in the past few years.[22−24] Other experiments also show a change in material glass transition temperature,[25] enhancement of shear viscosity at very low volume fractions of the dispersed particles,[26,27] and anisotropic yield stresses, thixotropy, and frozen memory.[28]

The underlying mechanism which controls this nonlinear viscoelastic behavior is mainly attributed to the breakage of the spatial structures created by the agglomerated particles, which are fused by electrostatic or van der Waals' forces.[23,29,30] However, particle surface treatment dramatically affects mac-

* Corresponding author. Tel: (803) 777-8022. Fax: (803) 777-0973. E-mail: jabbari@engr.sc.edu.

10.1021/bm050958s CCC: $33.50
Published on Web 04/07/2006

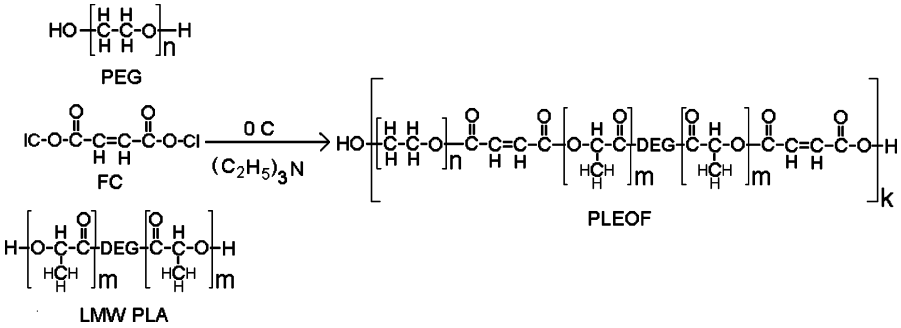

Figure 1. Schematic chemical structure of the poly(L-lactide-*co*-ethylene oxide-*co*-fumarate).

roscopic viscoelastic properties, which demonstrates the importance of thermodynamic interactions between the polymer chains and dispersed nanoparticles.[22,26,31] These two reinforcement mechanisms can be distinguished experimentally by their ability to restore the equilibrium values for storage modulus and viscosity after the cessation of deformation. It has been shown that the nonlinear viscoelastic behavior of the polymeric composites with agglomerated particle structures is followed by an irreversible change in microstructure. However, energetic interactions between the polymer chains and the surface of nanoparticles are reversible and the material is able to restore the original values of viscosity and elastic modulus after a finite deformation.[32]

Constitutive models to predict the macroscopic viscoelastic properties of polymer nanocomposites are still under development. When close-range filler−filler interactions dominate, phenomenological models of filler cluster breakdown and reagglomeration of particle networks appear to be adequate to describe most aspects of the observed nonlinear viscoelasticity.[29,33] A few continuum thermodynamics approaches are also proposed to capture the kinetics of floc evolution.[34,35]

Models for systems with strong energetic polymer−filler interactions are less developed.[36−38] Sarvestani and Picu recently developed a series of theoretical models for such systems in entangled and nonentangled regimes.[39,40] Although conceptually simple, their models capture the main features that distinguish nanocomposite and microcomposite behaviors. For example, the rubber-like response at low frequencies and the enhanced reinforcement at low deformation rates distinguish these behaviors. In their modeling approach however, it is assumed that all matrix chains equally contribute in the adsorption/desorption process to/from the nanoparticles. Thus, the role of free chains which are located far from the interaction zone, in close vicinity of the affine nanoparticles, is disregarded. In this paper, we relax this restrictive assumption by introducing a parallel kinetic equation for the free chains in addition to that of the adsorbed polymers. These sets of Langevin type equations are coupled by their fundamental relaxation times which are estimated by an activation model. The model has physically meaningful fitting parameters which include the characteristic energy of interaction between the two phases and the fraction of chains which contribute in attachment/detachments kinetics. A complete parametric study of the model is presented in a separate publication.[41]

Experimental Section

Synthesis and Characterization of Low Molecular Weight Poly(lactic acid) (LMW PLA). LMW PLA was synthesized by ring opening polymerization of L-lactide monomer (LA; Oretc, Inc., Easley, SC) in a dry atmosphere with diethylene glycol (DEG, Aldrich) as the initiator and tin octoate (TOC, Aldrich) as the polymerization catalyst.[42,43] The molar ratio of DEG to TOC was 25:1, and the molar ratio of LA to DEG was varied from 10 to 30 to produce LMW PLA with number average molecular weights (M_n) in the range of 1000−4000 Da. The synthesized LMW PLA was characterized by ^{1}H NMR and gel permeation chromatography (GPC). The LMW PLA had M_n and PI of 3.3 kDa and 1.6 based on GPC, respectively.

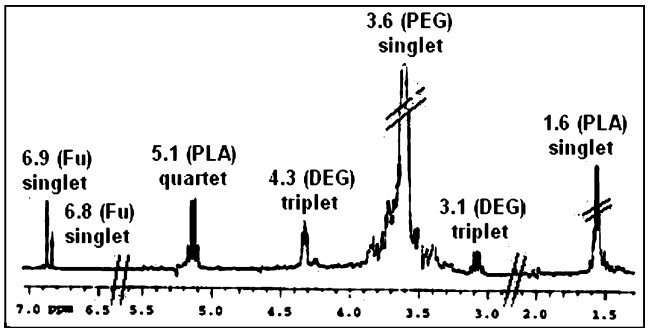

Figure 2. ^{1}H NMR spectrum of the PLEOF terpolymer.

Synthesis and Characterization of PLEOF Terpolymer. PLEOF was synthesized by condensation polymerization of LMW PLA and poly(ethylene glycol) (PEG; Aldrich) with fumaryl chloride (FuCl; Aldrich) and triethylamine (TEA; Aldrich) as the catalyst (Figure 1).[44,45] FuCl was purified by distillation at 161 °C, and PEG was dried by azeotropic distillation from toluene. The molar ratios of FuCl:PEG and TEA:PEG were 0.9:1.0 and 1.8:1.0, respectively. PLEOF terpolymer was synthesized using PEG and LMW PLA with M_n of 3.4 and 3.3 kDa, respectively. The weight ratio of PEG to PLA was 90:10 to produce a hydrophilic water-soluble terpolymer. In a typical reaction, 18 g of dried PEG and 2.0 g of LMW PLA were dissolved in 150 mL of methylene chloride under a dry nitrogen atmosphere in a three-neck reaction flask. The reaction vessel was placed in an ice bath to limit the temperature increase caused by the exothermic reaction. Next, 0.61 mL of FuCl and 1.55 mL of TEA, each dissolved in 15 mL of MC, were added dropwise to the reaction with stirring. After the addition of FuCl and TEA, the reaction was continued for 6 h under ambient conditions. After completion of the reaction, solvent was removed by rotovaporation, and the residue was dissolved in 300 mL of anhydrous ethyl acetate (Aldrich). The mixture was kept at 5 °C for 12 h for complete precipitation of the byproduct triethylamine hydrochloride and the salt was then removed by filtration. Ethyl acetate was removed by vacuum distillation, and the macromer was redissolved in MC and precipitated twice in ice cold ethyl ether. It was dried in a vacuum (less than 5 mmHg) at ambient temperature for at least 12 h and stored at −20 °C.

The structure of the PLEOF macromer was characterized by ^{1}H NMR and FTIR. Four singlet chemical shifts with peak positions at 1.6, 3.5, 6.8, and 6.9 ppm, two triplets with peaks positions at 3.6 and 4.2 ppm, and a quartet with peak position at 5.1 ppm were observed in the ^{1}H NMR spectrum of the terpolymer (Figure 2). The singlet chemical shift with peak position at 1.6 ppm was attributed to hydrogens of the methyl group (−CH_3) of the L-lactide monomer. The singlet chemical shift at

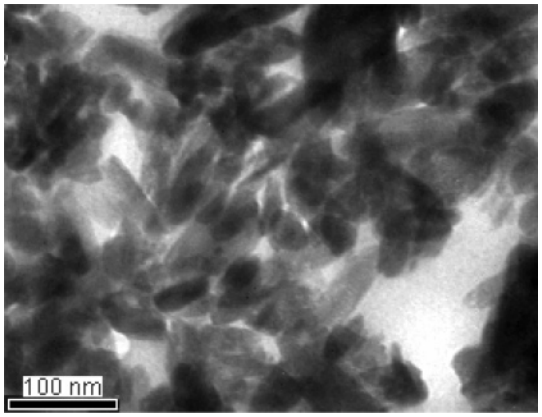

Figure 3. TEM micrograph of the bulk HA nanoparticles. Each primary nanoparticle has an ellipsoidal geometry with principal axes approximately equal to 80 and 20 nm.

3.5 ppm was attributed to the methylene hydrogens (CH_2-CH_2-O-) of ethylene oxide repeat units. The triplet chemical shifts centered at 3.6 and 4.2 ppm were due to the hydrogens of the methylene groups attached to the ether group ($-CH_2-O-CH_2-$) and the methylene groups attached to the lactide ester group (CH_2-OOC-), respectively, on the initiator DEG. The quartet chemical shift with peak position at 5.1 ppm was due to the hydrogen attached to the methine group of the lactide monomer. The singlet shifts at 6.90 and 6.95 ppm were attributed to the methine hydrogens of the fumarate in the middle of the chain ($-OOC-CH=CH-COO-$) and at chain ends ($-OOC-CH=CH-COOH$), respectively. The presence of peaks at 6.90 ppm in the NMR spectrum attributable to the hydrogens of the fumarate group, and the presence of a band due to the ester carbonyl stretching vibration centered at 1725 cm^{-1} in the FTIR spectra, confirmed the incorporation of fumarate monomers into the PLEOF macromer. The PLEOF macromer with PLA and PEG molecular weights of 3.3 kDa (PI of 1.6) and 3.4 kDa (PI of 1.3) had a M_n and PI of 18.3 kDa and 1.7, respectively, as determined by GPC.

PLEOF/Apatite Nanocomposite. HA nanoparticle whiskers were purchased from Berkeley Advanced Biomaterials (Berkeley, CA) and were used as the bioactive filler. HA nanoparticles tend to aggregate in bulk and form larger structures as shown in the TEM micrograph in Figure 3. The nanoparticles had an approximate ellipsoidal geometry with an aspect ratio equal to 4 where the principal axis was in the order of 80 nm (Figure 3). HA nanoparticles have surface hydroxyl groups and ionic carbonate and phosphate groups which have polar interactions with the PLEOF and form hydrogen bonds with the ether groups of PEO. The composite mixtures were prepared with apatite nanoparticle loading from 10 to 30 wt % of the final mixture, corresponding to volume fractions of 3 to 9% ($\rho_{HA} = 3.16$ g/cm^3). To prepare the mixtures, first HA nanoparticles were dispersed in 825 μL of distilled deionized water with vortexing. Next, 10 wt % PLEOF (31.5 mg) was dissolved in the suspension by vortexing and heating to 50 °C. The resulting dispersion was sonicated for 5 min with a 3 mm probe connected to an Ultrasonic Processor (model CP-130PB-1, Cole-Parmer Instruments, Vernon Hills, IL) with a power and frequency of 10 W and 20 kHz, respectively, in the continuous mode. Finally, the remaining 90 wt % of the PLEOF (283.5 mg) was added to the dispersion by heating to 50 °C with vortexing and sonicated again for 5 min. Sonication of the dispersion broke down the nanoparticle aggregates with concurrent attachment of the PLEOF chains to the surface of nanoparticles. The addition of a small fraction of PLEOF helped to stabilize the whiskers or smaller aggregates formed by sonication. The TEM micrograph in Figure 4b demonstrates that sonication breaks down large clusters (Figure 4a) into primary HA whiskers or smaller 100 nm size aggregates. The resulting dispersion was stable after one week.

Rheological Measurements. The viscoelastic characterization was done at 37 °C by a TA instrument AR2000 rheometer equipped with a cone and plate geometry (diameter: 20 mm; angle: 2°). The rheometer was mapped at extended precision due to low viscosity of the neat PLEOF samples without HA. The amplitude sweep measurements were done at the frequency of 1 Hz. In all cases, the samples were allowed to equilibrate for 20 min before measurements. The geometry was covered with a humidity chamber to prevent water evaporation from the dispersion during the experiment. The average value of five different measurements for each sample is reported. The results were repeatable with an average relative error of 15% for viscosity, storage and loss moduli (maximum error for highly filled samples and at slow/small deformations).

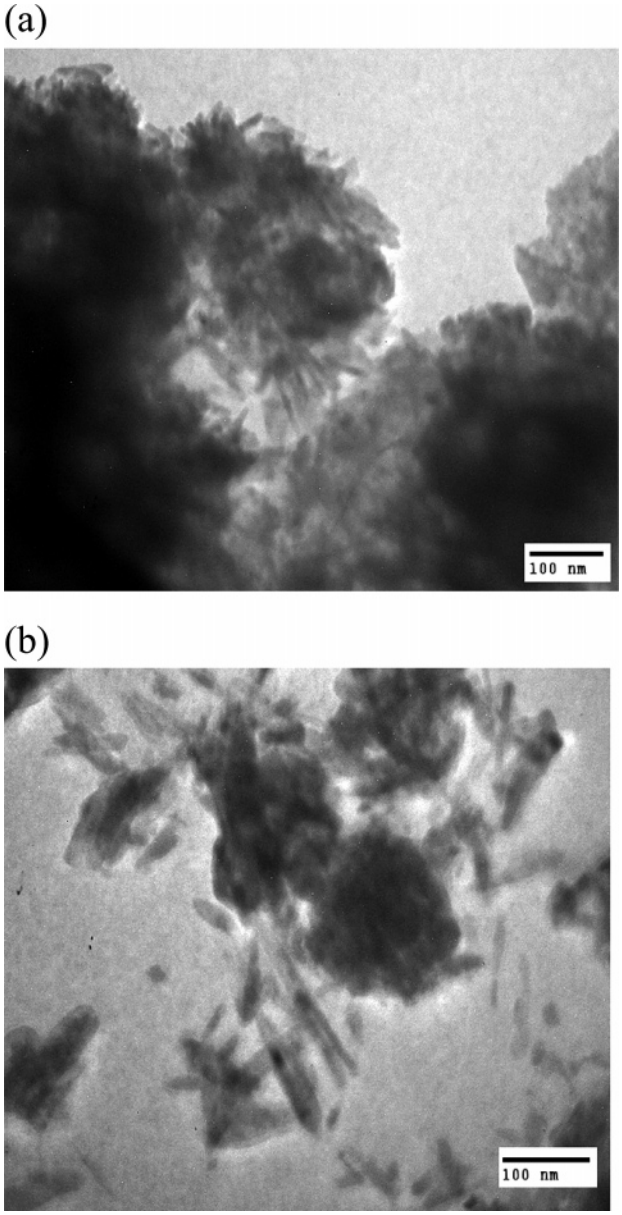

Figure 4. TEM micrograph of the state of dispersion before (a) and after (b) sonication.

Model

We used the linear elastic dumbbell model to describe the non-Newtonian rheological behavior of the filled PLEOF macromolecules. At any instant, a representative chain is either adsorbed to the surface of HA particle(s) or it is free. The total stress in the mixture is assumed to be the sum of stresses by free (σ^m) and adsorbed (σ^a) chains, i.e.

$$\sigma = \sigma^{m} + \sigma^{a} \tag{1}$$

Here, as an approximation, the stress production due to the short-range interparticle interactions within the aggregates is disregarded.

We start with the Maxwell (upper-convected) constitutive equations for the evolution of stress produced by the chains

$$\tau^{m}\hat{\boldsymbol{\sigma}}^{m} + \boldsymbol{\sigma}^{m} - G^{m}\mathbf{I} = 0 \tag{2a}$$

$$\tau^{a}\hat{\boldsymbol{\sigma}}^{a} + \boldsymbol{\sigma}^{a} - G^{a}\mathbf{I} = 0 \tag{2b}$$

where τ^i and G^i represent the corresponding relaxation time and modulus, respectively (i = a or m) and $\mathbf{I}$ is the identity tensor. Here, $\hat{\boldsymbol{\sigma}}$ designates the upper-convected derivative of stress tensor given by $\hat{\boldsymbol{\sigma}} = \partial\boldsymbol{\sigma}/\partial t - \boldsymbol{\sigma}\cdot(\nabla\upsilon) - (\nabla\upsilon)^{T}.\boldsymbol{\sigma}$, with υ being the velocity field. Obviously, one can utilize more elaborate constitutive equations, such as those proposed by Geisekus[46] and Larson,[47] which, contrary to the Maxwell equations, are able to predict the nonlinearity in the viscoelastic behavior of neat polymeric systems. However, PLEOF with M_n and PI of 6.3 kDa and 2.9, respectively, shows linear behavior almost in the entire range of deformation (rate) in an aqueous solution. Hence, we believe the observed nonlinearity in the behavior of filled systems is entirely due to the presence of nanoparticles and their interaction with the surrounding molecules, as it will be demonstrated in this paper.

Within the context of the dumbbell model, the relaxation times in eq 2 can be related to the chains diffusion coefficients and end-to-end distance as follows:

$$\tau^{m} = \frac{{R_0}^2}{6D^{m}} \tag{3a}$$

$$\tau^{a} = \frac{{R_0}^2}{6D^{a}} \tag{3b}$$

where D^i (i = a or m) and ${R_0}^2$ represent the chain diffusion coefficient and mean square end-to-end distance, correspondingly. Here, we have assumed that the adsorbed and free chains have an equal mean end-to-end distance. This assumption is supported by the recent molecular simulation studies.[48] Figure 5 shows the schematic configuration of a PLEOF chain adsorbed on the outer surface of a small HA aggregate. Using a coarse grained model, the structure of the adsorbed chain can be represented by connected (spherical) statistical segments which are either free or attached to the surface of nanoparticle. The attraction between the polymer and surface of nanoparticles (through hydrogen bonding or polar interactions) affects the chain dynamics. To quantify this effect, the polymer−particle energetic affinity is modeled as a frictional interaction between the adsorbed bead and particle surface, in addition to the regular inter-bead friction. Therefore, the total friction coefficient in the hydrodynamic force acting on the adsorbed bead (ith bead) is[40]

$$(\xi)_i = \xi_{ad}, \; i\text{th bead is adsorbed} \tag{4a}$$

$$(\xi)_i = \xi_0, \; i\text{th bead is not adsorbed} \tag{4b}$$

where ξ_{ad} is the friction coefficient due to polymer-particle interaction and ξ_0 represents the friction coefficient corresponding to the self-diffusion of a single bead and accounts for its friction with the solvent molecules and/or other nonbonded polymer beads. Using a simple activation model[49] for a bead

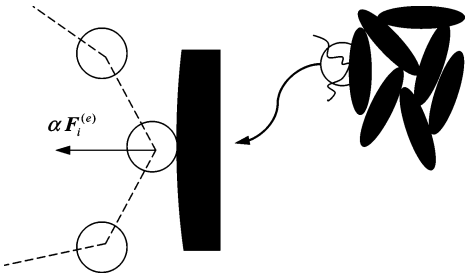

Figure 5. Schematic diagram of the attached section of an adsorbed PLEOF chain using a coarse grained model. The ith bead is attached and the two beads located at the immediate neighborhood pull the attached bead by entropic forces equal to $F_i^{(e)}$. The resultant force exerted on the attached bead is $F_i^{(e)}$.

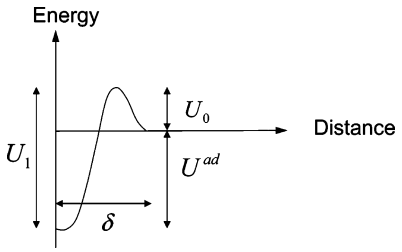

Figure 6. Description of the various potential energy barriers used by the proposed activation model.

of size a, this friction coefficient is approximated by $\xi_0 = 2k_BT\tau_0/a^2$, with the time constant τ_0 being

$$\tau_0 = \tau^* \exp\left(\frac{U_0}{k_BT}\right) \tag{5}$$

where k_BT is the thermal energy. Here $\tau^* \sim a(m/k_BT)^{1/2}$ is the characteristic time of the molecular vibrations, U_0 is the activation energy for diffusion of a segment in the bulk, and m is its mass.

ξ_{ad} can be estimated by a similar thermal activation model. The friction due to the attachment is given by $\xi_{ad} = 2k_BT\tau_{ad}/a^2$, where the time constant of detachment, τ_{ad}, is defined as

$$\tau_{ad} = \tau^* \exp\left(\frac{U_1 - \alpha F_i^{(e)}\delta}{k_BT}\right) \tag{6}$$

Here $\tau^* \sim a(m/k_BT)^{1/2}$ again stands for the inverse of the detachment attempt frequency, and U_1 is the required energy to detach the adsorbed bead from the filler surface (Figure 6). $F_i^{(e)}$ is the entropic force between two consecutive beads. In eq 6, it is acknowledged that the detachment process is favored by the resultant tension $\alpha F_i^{(e)}$ ($2 \geq \alpha \geq 0$) exerted on the adsorbed bead by the adjacent strands (Figure 5). δ is an activation length on the order of the displacement required to move the bead from the layer next to the surface of the filler into the neighboring bulk (Figure 6).

Next, this activation theory is implemented in the adopted dumbbell model. Making a mean-field type approximation, we assume that the probability of bead-particle attachment is constant along the chain. Therefore, the representative chain has constant friction ξ_{ad} along its contour. We take ξ^m and ξ^a to be the friction coefficients corresponding to the free and adsorbed dumbbells, respectively. Since the hydrodynamic friction coefficient is inversely proportional to the diffusion coefficient (fluctuation−dissipation theorem), from (5) and (6), we can write

$$\frac{D^{m}}{D^{ad}} = \exp\left(\frac{U^{ad} - \alpha F^{a}\delta}{k_B T}\right) \quad (7)$$

Here, U^{ad} is evaluated as the energy difference of a bead residing on a filler surface and its energy in the bulk; i.e., $U^{ad} = U_1 - U_0$ (Figure 6). In addition, F^{a} stands for the entropic force in an adsorbed elastic dumbbell. Therefore, from eqs 3 and 7, we have

$$\tau^{a} = \tau^{m} \exp\left(\frac{U^{ad} - \alpha F^{a}\delta}{k_B T}\right) \quad (8)$$

The rate of adsorption and desorption can be shown by a simple kinetic equation

$$\frac{dN^{a}}{dt} = \bar{N}^{m}(\tau_0)^{-1} - N^{a}(\tau_{ad})^{-1} \quad (9)$$

where N^{a} shows the number density of adsorbed dumbbells and $\bar{N}^{m}$ represents the number density of free dumbbells which are located close enough to the surface of the nanoparticles and can contribute in an adsorption−desorption process. According to the classical theory of rubber elasticity, a linear dependency is introduced between the modulus and number density of the chains at constant temperature; i.e., $G^{i} \propto N^{i}$. Thus, in steady-state situation

$$\frac{G^{a}}{\bar{G}^{m}} = \exp\left(\frac{U^{ad} - \alpha F^{a}\delta}{k_B T}\right) \quad (10)$$

$\bar{G}^{m}$ designates the modulus of free chains located close to the surface of the nanoparticles and it is different from G^{m}, the modulus of free chains located in the bulk. The relation between G^{m} and the modulus of the corresponding neat polymer solution, $G°$, follows the well-known Einstein equation for the hydrodynamic contribution of the solid phase with low volume fraction ϕ, i.e.

$$G^{m} = G°\,(1 + 2.5\phi) \quad (11)$$

Here, we have assumed that the aggregated HA nanoparticles have monodisperse spherical shape on average with volume fraction ϕ, below the corresponding percolation threshold.

The contribution of polymer molecules to the stress tensor is given by Kramers expression

$$\boldsymbol{\sigma}^{m} = 3G^{m}\frac{\langle \mathbf{R}^{m}\mathbf{R}^{m}\rangle}{R_0^{\,2}} \quad (12a)$$

$$\boldsymbol{\sigma}^{a} = 3G^{a}\frac{\langle \mathbf{R}^{a}\mathbf{R}^{a}\rangle}{R_0^{\,2}} \quad (12b)$$

where $\mathbf{R}^{i}$ (i = a or m) is the dumbbell end-to-end vector and $\langle\cdots\rangle$ shows the ensemble average. Note that the linear elastic force in an adsorbed dumbbell is $F^{a} = 3k_B T R^{a}/R_0^{2}$. Taking advantage of eq 12b it can also be shown as $F^{a} = k_B T/R_0(3tr\boldsymbol{\sigma}^{a}/G^{a})^{1/2}$.

It is noteworthy that the adopted linear elastic dumbbell model can be readily extended to classical Rouse model by incorporating a simple modal analysis for the chain relaxation. Within this framework, the stress contributed by the pth mode is[50]

$$\sigma_p = \sigma_p^{m} + \sigma_p^{a} \quad (13)$$

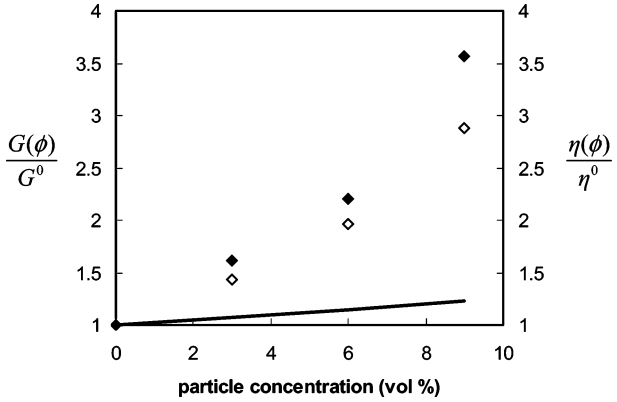

Figure 7. Comparison of the experimental results for $G(\phi)/G°$ (full symbols) and $\eta(\phi)/\eta°$ (open symbols) with Einstein equation (solid line).

where

$$\sigma_p^{m} = 3G^{m}\frac{\langle \mathbf{R}_p^{m}\mathbf{R}_p^{m}\rangle}{R_0^{\,2}} \quad (14a)$$

$$\sigma_p^{a} = 3G^{a}\frac{\langle \mathbf{R}_p^{a}\mathbf{R}_p^{a}\rangle}{R_0^{\,2}} \quad (14b)$$

The corresponding Maxwell equations for the evolution of these stress components are

$$\tau_p^{m}\hat{\boldsymbol{\sigma}}_p^{m} + \boldsymbol{\sigma}_p^{m} - G^{m}\mathbf{I} = 0 \quad (15a)$$

$$\tau_p^{a}\hat{\boldsymbol{\sigma}}_p^{a} + \boldsymbol{\sigma}_p^{a} - G^{a}\mathbf{I} = 0 \quad (15a)$$

where the total stress tensor is $\sigma = \sum_p \boldsymbol{\sigma}_p$. The modal relaxation times in eq 14 are $\tau_p^{i} = \tau_{Rouse}^{i}/p^2$ with $\tau_{Rouse}^{i} = R_0^{2}/12\pi^2 D^{i}$ (i = a or m).

Results and Discussion

We examine the predictions of the proposed model for the steady state simple shear response of the PLEOF/HA nanocomposites. These predictions are compared with the results of the experimentally measured shear viscosity and storage modulus of the filled systems as well as the neat polymer solutions. The shear viscosity and storage modulus of a series of samples with increasing content of HA nanoparticles were measured, and the results were compared with the model predictions. The observations for the flow curve and amplitude sweep are shown and discussed in this paper. Similar tests are performed on the nonfilled PLEOF solution to have a base for comparison when discussing the effect of nanoparticles reinforcement.

τ^{a}/τ^{m}, $\epsilon = \exp(U^{ad}/k_B T)$, and δ/R_0 are the model parameters which represent the nature of the energetic interactions between the PLEOF chains and HA nanoparticles and therefore they are constant for all filled samples. Other fitting parameters are $G^{a}/G°$ and $\bar{G}^{m}/G°$ which are proportional to the number of the adsorbed chains and those free chains which are located in close vicinity of the HA particles and contribute to the adsorption−desorption kinetics. Hence, these two parameters change with the concentration of nanoparticles. Only the viscosity results as a function of shear rate in Figure 8 was used for parameter fitting. The best fit of the experimental results to the model for the neat polymer was obtained with $G° = 11.65$ Pa and $\tau^{m} = 0.46$ s. Other extracted fit parameters are listed in Table 1.

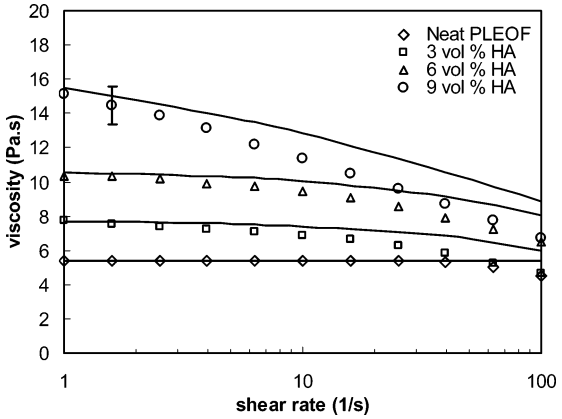

Figure 8. Model results (solid line) for the shear viscosity vs shear rate compared with the experimental data (points). The error bars show the standard deviation of the experimental data at slow deformations only for the samples with 9 vol % HA.

Table 1. Fit Parameters of the Proposed Model for PLEOF/HA Nanocomposites[a]

parameters independent from filler concentration		
$\tau^a/\tau^m = 7.13$	$\epsilon = 10$	$\delta/R_0 = 0.1$

parameters variable with filler concentration		
ϕ	G^a/G°	$\bar{G}^m/G^\circ$
3 vol %	0.05	0.007
6 vol %	0.11	0.02
9 vol %	0.26	0.04

[a] The represented values of the concentration dependent parameters correspond to the low shear rate or low amplitude regimes.

It is instructive to compare the observed values for zero shear viscosities and low amplitude storage moduli with the predictions of continuum theories such as the well-known Einstein equation for suspension of spherical particles

$$\frac{G(\phi)}{G^0} = \frac{\eta(\phi)}{\eta^0} = 1 + 2.5\phi \qquad (16)$$

$G(\phi)$ and $\eta(\phi)$stand for the low amplitude storage modulus and zero shear viscosity of the composite, respectively. Figure 7 reveals a very large difference between our experimental results and the predictions of eq 16, where the experiments show far larger values for reduced modulus and viscosity. This discrepancy is rooted in the assumption of the continuum viscoelasticity theory for colloidal suspensions that the size of suspended particles is much bigger than the characteristic length scale of the suspending medium. Hence, the reinforcement mechanism is solely due to the hydrodynamic interaction between the solid and liquid phases. This assumption ceases to be valid when the average size of the particle aggregates becomes comparable with the average size of the chains. In this situation, the majority of the chains in the suspending medium have the opportunity to be adsorbed by the solid surface, where in the corresponding case of particles with much larger size (at the same volume fraction) the adsorbed molecules are limited within a boundary layer around each particle having a negligible fraction.

The dependence of the steady shear viscosity, η, on shear rate measured at different concentrations of HA nanoparticles is shown in Figure 8 along with the model predictions. While the neat PLEOF solution exhibits shear rate independency almost within the entire range of the applied shear rate, the filled systems show a non-Newtonian shear thinning behavior. In addition, the onset of shear thinning shifts toward the lower shear rates as the concentration of nanoparticles increases. Ultrasonication of the dispersion minimizes the effect of the breakage of local particle aggregates on the material viscoelasticity. For this reason, it is conjectured that the observed viscoelastic nonlinearity may be due to the polydispersity in the relaxation time of the macromolecules. Using a simplified approach, this is incorporated in our model by introducing another relaxation time, τ^a, for the adsorbed chains, which is longer than τ^m, the relaxation time of the free chains (see eq 8). Relaxation time τ^a is not constant and decreases as the chain entropic force increases with deformation (rate).

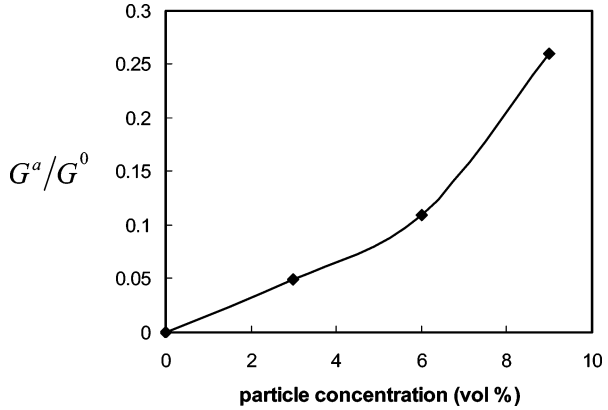

Figure 9. Normalized modulus of the adsorbed chains, G^a/G°, as a function of the filler concentration. G^a is proportional to the number density of adsorbed chains (N^a).

At higher volume fractions of the nanoparticles, the effective outer surface area of the solid phase increases, and therefore, the number of adsorbed chains with slower relaxation times increases, resulting in the enhancement of the overall viscosity of the system. Figure 9 shows the model prediction for the ratio G^a/G^0 at different volume fractions of the nanoparticles, which is an indicator of the normalized number density of adsorbed chains.

Samples were also subjected to repetitive dynamic strain amplitude sweep at a constant frequency of 1 Hz. Figure 10 shows the measurements for storage (G') and loss modulus (G'') vs amplitude of oscillation. As expected, although the pure PLEOF shows an amplitude independent viscoelastic behavior over the entire range of the applied strain, the storage and loss moduli of the filled systems decrease after a low amplitude linear viscoelastic range. Again, the value of the strain corresponding to the end of the linear viscoelastic regime shifts toward the lower values as the HA particle concentration increases.

We believe that the reduction of storage and loss moduli in our experimental results cannot be solely due to the breakdown of the cluster of fused nanoparticles. As pointed out earlier, the clusters of the fused nanoparticles in the dispersion have disintegrated into smaller aggregates by sonication before the application of deformation (Figure 4). It is unlikely that these aggregates can disintegrate into smaller units under the studied range of deformations. To prove this, we repeated the amplitude sweep test on the samples with a relaxation period between the two runs. It turns out that the material is almost able to restore the low amplitude values for storage modulus in the second run, which indicates that the observed nonlinearity is due to a reversible process. As an example, the rheological responses for the two consecutive amplitude sweeps on the same sample with 9 vol % nanoparticles are compared in Table 2. Our proposed model is able to describe this nonlinear viscoelastic phenomena based on the dynamics of the reversible stick/slip

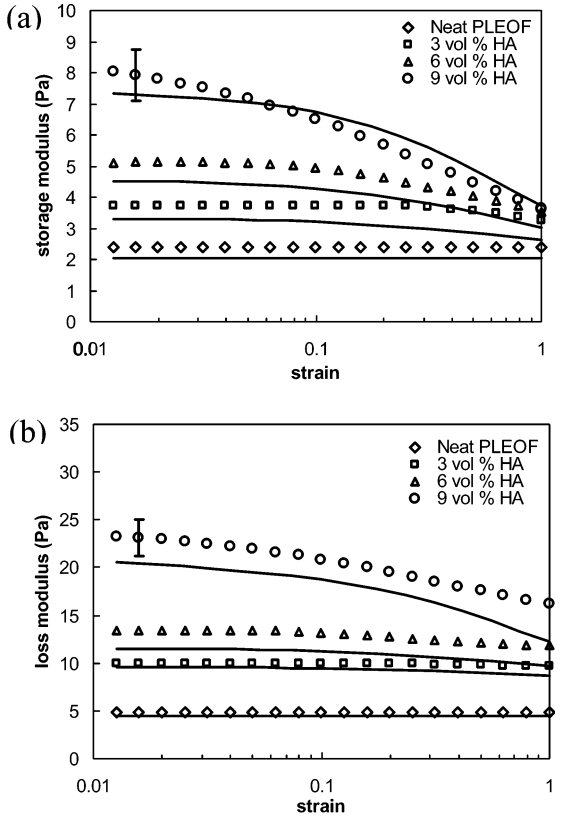

Figure 10. Model results (solid line) for the storage (a) and loss modulus (b) vs amplitude compared with the experimental data (points). The error bars show the standard deviation of the experimental data at small deformation only for the samples with 9 vol % HA.

Table 2. Measured Storage Modulus of PLEOF/HA Nanocomposite (9 vol %) Obtained from Two Consecutive Amplitude Sweeps[a]

	storage modulus (Pa)					
strain	0.013	0.031	0.079	0.199	0.500	1.000
first run	8.116	7.524	6.672	5.648	4.524	3.7216
second run	7.301	6.926	6.312	5.289	4.081	3.184

[a] The sample was allowed to equilibrate for 30 min before the second run.

process of adsorbed chains on the surface of the nanoparticles. The model predictions for the strain dependence of the storage and loss modulus, using the fitting parameters obtained from the viscosity data in Figure 8 (see Table 1) are shown in Figure 10 along with the experimental results.

Although the model's predictions reasonably match with experimental data in dilute systems, it turns out that there are discrepancies between these data and respective theoretical predictions in more concentrated samples. It should be noted that the preparation of mixtures with well-dispersed aggregates of small size is more difficult when the concentration of the solid phase increases. In such circumstances, the tendency for clustering of aggregates would be favored as the distance between them decreases. The growth in the HA nanocrystalline structure can be a result of the interparticle electrostatic or van der Waals' forces as well as the topotactic oriented attachment of primary particles at high energy surfaces of the nanocrystals in hydrothermal conditions.[51]

The observed discrepancy can also be attributed to the simplicity of our activation model for the attachment/detachment kinetics. Contrary to the simplifying assumption of equal residence time for all of the adsorbed chains, in reality, macromolecules may be adsorbed to the surface of nanoparticles at different number of attachment points. Those first chains which come in contact with the filler see the whole free surface and can get a strong bond to the particle at many points and form a strongly adsorbed layer on the particles. Chains which arrive at the surface at later times find the area widely covered and may be adsorbed only at isolated free sites and form weaker links to the surface.[36]

Conclusions

We have studied the rheological behavior of the aqueous dispersions of PLEOF containing HA nanoparticles. After cross-linking, these resorbable composites are useful as a bioactive bone substitute. Experimental results on the steady-state shear viscosity as well as storage modulus in strain sweep show a nonlinear viscoelasticity in material behavior, where the degree of nonlinearity increases with the concentration of the dispersed HA nanoparticles. The nonlinear viscoelasticity in our experimental results is rooted in the energetic interactions between the PLEOF chains and HA nanoparticles through the hydrogen bonds between the PEO blocks and the polar groups on the surface of HA. With reduction of the size of the dispersed particles at a constant volume fraction, an enormous surface area of the solid phase is exposed to the surrounding chains. As a result of the energetic interactions between the two phases, a large fraction of the polymer chains adsorb to the surface of nanoparticles. This increases the corresponding relaxation time of the adsorbed chains resulting in the enhancement of continuum properties such as viscosity and storage modulus. We proposed an activation model for the lifetime of reversible polymer-particle attachment points. The model implies that the attachment lifetime is a function of its adsorption energy and it varies with the entropic force exerted by the polymer segment at the attachment point. Therefore, the nonlinearity is controlled by the amplitude of deformation as well as the deformation rate compared with the kinetic rate of adsorption−desorption process.

A linear elastic dumbbell model is proposed to predict the viscometric properties of the nanocomposite at the macroscopic scale. Our model predicts a reduction in viscosity and modulus with increasing shear rate and strain, respectively, while there is discrepancies in the values at higher deformation (rate) especially for more concentrated systems. This is most likely due to the simple kinetic model that we have adopted for the dynamics of adsorption and desorption. In addition, at higher volume fractions of the dispersed particles, there is greater probability of finding bigger clusters of particles after the sonication. Hence, the discrepancy, in part, can be attributed to the breakdown of larger aggregates.

References and Notes

(1) Jabbari, E.; Lu, L.; Yaszemski, M. J. In: *Handbook of biodegradable polymeric materials and their applications*; Mallapragada, S. K., Narasimhan, B., Eds.; American Scientific Publishers: Stevenson Ranch, CA, 2004; Vol. 2.
(2) Helm, G. A.; Dayoub, H.; Jane, J. A. *Neurosurg. Focus.* **2001**, *10*, 1.
(3) Jabbari, E.; Lu, L.; Currier, B. L.; Mikos, A. G.; Yaszemski, M. J. In: *Tissue engineering in musculoskeletal clinical practice*; Sandell, L. J., Grodzinsky, A. J., Eds.; American Academy of Orthopaedic Surgeons. Rosemont, IL, 2004, Chapter 32.
(4) Jabbari, E.; Wang, S.; Lu, L.; Gruetzmacher, J. A.; Ameenuddin, S.; Hefferan, T. E.; Currier, B. L.; Windebank, A. J.; Yaszemski, M. J. *Biomacromolecules* **2005**, *6*, 2503.

(5) Brown, R. Q.; Mount, A.; Burg, K. J. *J. Biomed. Mater. Res. A.* **2005**, *1*, 74, 32.
(6) Declercq, H. A.; Gorski, T. L.; Tielens, S. P.; Schacht, E. H.; Cornelissen, M. J. *Biomacromolecules* **2005**, *6*, 1608.
(7) Trojani, C.; Weiss, P.; Michiels, J. F.; Vinatier, C.; Guicheux, J.; Daculsi, G.; Gaudray, P.; Carle, G. F.; Rochet, N. *Biomaterials* **2005**, *26*, 5509.
(8) Sittinger, M.; Hutmacher, D. W.; Risbud, M. V. *Curr. Opin. Biotechnol*. **2004**, *15*, 411.
(9) Gao, J.; Dennis, J. E.; Solchaga, L. A.; Goldberg, V. M.; Caplan, A. I. *Tissue Eng.* **2002**, *8*, 827.
(10) Joosten, U.; Joist, A.; Frebel, T.; Walter, M.; Langer, M. *J. Hand Surg.* **2000**, *25B*, 288.
(11) Rodrigues, C. V. M.; Serricella, P.; Linhares, A. B. R.; Guerdes, R.; Borojevic, R.; Rossi, M. A.; Duarte, M. E. L.; Farina, M. *Biomaterials* **2003**, *24*, 4987.
(12) Damien, E.; Hing, K.; Saeed, S.; Revell, P. A. *J. Biomed. Mater. Res. A.* **2003**, *66A*, 241.
(13) Hu, Y.; Zhang, C.; Zhang, S.; Xiong, Z.; Xu, J. *J. Biomed. Mater. Res. A.* **2003**, *67A*, 591.
(14) Jabbari, E.; Gruetzmacher, J. A.; Lu, L.; Currier, B. L.; Yaszemski, M. J. *Polym. Preprints* **2003**, *44*, 184.
(15) Jabbari, E.; He X. *Proc. Annual AIChE Conf.*; American Institute of Chemical Engineers: Cincinnati, OH, 2005; p 159.
(16) Jabbari, E.; Muthukumarasamy Ayyadurai, S. *Proc. Annual AIChE Conf.*; American Institute of Chemical Engineers: Cincinnati, OH, 2005; p 108.
(17) Jabbari, E. *Proc. Annual AIChE Conf.*; American Institute of Chemical Engineers: Cincinnati, OH, 2005; p 159.
(18) Roether, J. A.; Deb, S. *J. Mater. Sci. Mater. Med*. **2004**, *15*, 413.
(19) Harper, E. J.; Braden, M.; Bonfield, W. *J. Mater. Sci. Mater. Med.* **2000**, *11*, 491.
(20) Jabbari, E. *MRS Proceedings*; Materials Research Society: Boston, MA, 2005; p 144.
(21) Payne, A. R. In *Reinforcement of elastomers*; Kraus, G., Ed.; Interscience: New York, 1965; p 69.
(22) Aranguren, M. I.; Mora, E. M.; DeGroot, J. V.; Macosko, C. W. *J. Rheol.* **1992**, *36*, 1165.
(23) Cassagnau, Ph. *Polymer* **2003**, *44*, 2455.
(24) Harzallah, O. A.; Dupuis, D. *Rheo. Acta* **2003**, *42*, 10.
(25) Berriot, J.; Montes, H.; Lequeux, F.; Long, D.; Sotta, P. *Macromolecules* **2002**, *35*, 9756.
(26) Zhang, Q.; Archer. L. A. *Macromolecules* **2004**, *37*, 1928.
(27) Reynaud, E.; Jouen, T.; Gauthier, C.; Vigier, G.; Varlet J. *Polymer* **2001**, *42*, 8759.
(28) Leonov, A. I. *J. Rheol.* **1990**, *34*, 1039.
(29) Heinrich, G.; Klüppel, M. *Adv. Polym. Sci*. **2002**, *160*, 1.
(30) Cassagnau, Ph.; Mélis, F. *Polymer* **2003**, *44*, 6607.
(31) Zhang, Q.; Archer, L. A. *Langmuir* **2002**, *18*, 10435.
(32) Osman, M. A.; Atallah, A. *Polymer* **2005**, *46*, 9476.
(33) Wolthers, W.; van den Ende, D.; Breedveld, V.; Duits, M. H. G.; Potanin, A.; Wientjes, R. H. W.; Mellema, J. *Phys. Rev. E* **1997**, *56*, 5726.
(34) Sobhanie, M.; Isayev, A. I. *J. Non-Newtonian Fluid Mech.* **1999**, *85*, 189.
(35) Leonov, A. I. *J. Rheol*. **1990**, *34*, 1039.
(36) Maier, P. G.; Göritz, D. *Kautsch. Gummi Kumstst*. **1996**, *49*, 18.
(37) Simhambhatla, M.; Leonov, A. I. *Rheol. Acta* **1995**, *34*, 329.
(38) Havet, G.; Isayev, A. I. *Rheol. Acta* **2001**, *40*, 570.
(39) Sarvestani, A. S.; Picu, C. R. *Polymer* **2004**, *45*, 7779.
(40) Sarvestani, A. S.; Picu, C. R. *Rheol. Acta* **2005**, *61*, 132.
(41) Jabbari, E.; Sarvestani, A. S. *Macromol. Theory Simul*. **2005**, submitted.
(42) Dechy-Cabaret, O.; Martin-Vaca, B.; Bourissou, D. *Chem. Rev.* **2004**, *104*, 6147.
(43) Jabbari, E. *Proc. Int. Symp. Microencapsulation* **2003**, 54.
(44) Jabbari, E.; Muthukumarasamy Ayyadurai, S. *Proc. Annual AIChE Conf.*; American Institute of Chemical Engineers: Cincinnati, OH, 2005; p 108.
(45) Jabbari, E. *Proc. Annual AIChE Conf.*; American Institute of Chemical Engineers: Cincinnati, OH, 2005; p 95.
(46) Giesekus, H. *J. Non-Newtonian Fluid Mech*. **1982**, *11*, 69.
(47) Larson R. G. *J. Non-Newtonian Fluid Mech*. **1983**, *13*, 279.
(48) Picu, R. C.; Ozmusul, M. S. *J. Chem. Phys*. **2003**, *118*, 11239.
(49) Frenkel, J. *Kinetic theory of liquids*; Clarendon: Oxford, U.K.,1946.
(50) Marrucci, G.; Ianniruberto, G. *Chem. Eng. Sci.* **2001**, *56*, 5539.
(51) Penn, R. L.; Banfield, J. F. *Geochim. Cosmochim. Acta* **1999**, *63*, 1549.

BM050958S